Carbohydrate Polymers 105 (2014) 214–221

Contents lists available at ScienceDirect

Carbohydrate Polymers

journal homepage: www.elsevier.com/locate/carbpol

Investigation of the scaling law on gelation of oppositely charged nanocrystalline cellulose and polyelectrolyte

Ang Lu[a,b], Yixiang Wang[c], Yaman Boluk[a,d,*]

[a] Department of Civil and Environmental Engineering, University of Alberta, Edmonton, Alberta T6G 2G2, Canada
[b] Department of Chemistry, Wuhan University, Wuhan, 430072, China
[c] Department of Agricultural, Food and Nutritional Science, University of Alberta, Edmonton, Alberta T6G 2P5, Canada
[d] National Institute for Nanotechnology, National Research Council of Canada, Edmonton, Alberta T6G 2M9, Canada

ARTICLE INFO

Article history:
Received 14 December 2013
Received in revised form 13 January 2014
Accepted 22 January 2014
Available online 31 January 2014

Keywords:
Nanocrystalline cellulose
Gelation
Opposite charge

ABSTRACT

The sol–gel transition in the mixture system of oppositely charged polyelectrolyte (quaternized hydroxyethylcellulose ethoxylate, QHEC) and nanocrystalline cellulose (NCC) induced by electrostatic adsorption interaction was investigated by rheological means. Winter and Chambon theory was validated to be applicable for the critical gel point determination, and critical gel point have been successfully determined. With QHEC concentration increasing, more NCC were needed to form a critical gel, and smaller loss tangent and relaxation exponent (n) values at the gel point were observed, indicating the elastic nature of mixture was enhanced with QHEC increase. Gel strength behaved as a function of both QHEC and NCC concentrations, suggesting the gel network at the critical point was composed of entanglements and association of QHEC macromolecular chains, as well as the electrostatic adsorption interaction between QHEC chains and NCC rods. The calculated number of NCC rods per junction decreased from 0.30 to 0.01 when the QHEC concentration increased from 1.0 wt% to 3.0 wt%, indicating the electrostatic adsorption interaction between the NCC rods and QHEC chains was less significant to gel formation at higher QHEC concentrations. Therefore, the exponents of scaling law $\eta_0 \propto \epsilon^{-\gamma}$ and $G_e \propto \epsilon^{z}$ for the QHEC/NCC mixtures revealed that the scaling law $n = z/(z+\gamma)$ between n, γ, and z was only feasible at highest QHEC concentration, since the intermolecular interaction (electrostatic adsorption interaction in this article) was so weak that can be neglected and the critical gel network was dominated by QHEC chain entanglements and association.

1. Introduction

Nanocrystallines cellulose (NCC) is the fundamental constitutive polymeric motif of macroscopic cellulosic-based fibers, and can be extracted by acid hydrolysis of cellulosic materials, such as bacteria cellulose, cotton, and wood pulp (Habibi, Lucia, & Rojas, 2010; Moon, Martini, Nairn, Simonsenf, & Youngblood, 2011; Rånby, 1949; Liu et al., 2011). This rod-shaped material has attracted a lot of attention over the past several decades because of its availability, renewability, light weight, nano-scale dimension, unique morphology and low cost (Habibi et al., 2010). Therefore, NCC has been widely employed as reinforcing agent in nanocomposites (Samir, Alloin, & Dufresne, 2005; Siro & Plackett, 2010), barrier membranes (Siqueira, Bras, & Dufresne, 2010; Paralikar, Simonsen, & Lombardi, 2008), packing materials (Yang, Tejado, Alam, Antal, & van de Ven, 2012; Azeredo, 2009; Rhim, 2007), biomedicines (Czaja, Young, Kawecki, & Brown, 2007; Liang, Hsiao, & Chu, 2007; Woltman, Jay, & Crawford, 2007), optically and electrooptically variable materials (Beck, Bouchard, & Berry, 2011; Pan, Hamad, & Straus, 2010), bioimaging (Dong & Roman, 2007), sensors (Nielsen, Eyley, Thielemans, & Aylott, 2010), catalysts (Benaissi, Johnson, Walsh, & Thielemans, 2010; Shin, Blackwood, Bae, Arey, & Exarhos, 2007) and so forth.

Systems consisted of oppositely charged colloids and polyelectrolytes exhibited complex self-aggregation behaviors (Pickrahn, Rajaram, & Mohraz, 2010; Hoffmann et al., 2011; Kumar, Dubin, Hernon, Li, & Jaeger, 2007). The structures formed by oppositely charged macroions and polyelectrolytes vary in a large dimension range, with respect to the detailed structural organization, and such mixtures have many applications, for examples in cosmetics, paints, detergency, and drug delivery (Hoffmann et al., 2011; Wang & Roman, 2011a; Wang & Roman, 2011b; Sivakumar et al., 2009; Yap, Quinn, Ng, Cho, & Caruso, 2005; Ye, Tong, & Fetters, 1997). Therefore, they have attracted quite some interest in the past decades (Lam & Walker, 2010; Bain et al., 2010; Mezei & Meszaros, 2008). Over a finite range of polyelectrolyte and colloid concentrations, polymer-induced bridging may result in a rheological sol–gel transition (Otsubo, 1990; Larson, 1999). Colloidal

* Corresponding author. Tel.: +1 780 492 6295.
E-mail address: yaman.boluk@ualberta.ca (Y. Boluk).

0144-8617/$ – see front matter © 2014 Elsevier Ltd. All rights reserved.
http://dx.doi.org/10.1016/j.carbpol.2014.01.077

gels formed in this way are frequently used as precursor inks for direct-write assembly of complex 3 dimensional structures with applications in advanced ceramics, sensors, and composites (Smay, Gratson, & Shepherd, 2002a; Smay, Cesarano, & Lewis, 2002b; Li & Lewis, 2003). Moreover, a remarkable attribute of the gels that make them excellent candidates for the applications is the ability to tune their rheological properties such as the zero-shear storage modulus, yield stress, and steady shear viscosity, over a relatively wide range. Therefore, a thorough understanding of the relationship between rheological transitions and microstructural changes will further advance our ability to engineer particulate materials with prescribed properties and can impact technologies ranging from food processing (Dickinson, 1992) to microfluidic separations (George et al., 2009), direct-write assembly (Smay et al., 2002a), and microextrusion (Wang, Shaw, & Cameron, 2006).

In the present paper, we investigate the gelation behavior in a mixture system composed of oppositely charged nanocrystalline cellulose (NCC) colloid suspension and polyelectrolyte (quaternized hydroxyethylcellulose ethoxylate, QHEC) aqueous solution, which was induced by the electrostatic attraction, as well as the rheological properties and scaling law application. Moreover, the microstructure and dynamics at the gel point have been as demonstrated. We hope to provide useful fundamental information on the interactions between oppositely charged colloids and polyelectrolyte, as well as the sol–gel transition behaviors, to promote the development of colloids/polymer composite materials.

2. Experimental section

2.1. Materials

Cationic polyelectrolyte quaternized hydroxyethylcellulose ethoxylate (QHEC) was purchased from Sigma–Aldrich (St. Louis, MO, USA) (Sameer Dalvi & Rajesh Dave., 2009). Lyophilized nanocrystalline cellulose (NCC) particles were supplied by Alberta Innovates Technology Futures (Edmonton, Alberta, Canada). The fabrication procedure was as follows: NCC particle sample was prepared by acid hydrolysis of commercial dissolved softwood pulp. Pulp was hydrolyzed with 64% sulfuric acid at 50 °C for 40 min, and then diluted with de-ionized water to stop the reaction. The suspension was then centrifuged, neutralized with Na_2CO_3 and dialyzed to remove the salts. Finally, the suspension was further dispersed in an ultrasonic bath to achieve 1–2% concentration stable colloidal suspension. NCC particles were obtained in powder form by lyophilizing the suspensions. Detailed preparation method was discussed elsewhere (Bondeson, Mathew, & Oksman, 2006; Boluk, Zhao, & Incani, 2012). NCC particles in aqueous solutions carried negative electrical charges due to the sulfate surface groups. All materials were used without further purification.

2.2. Samples preparation

QHEC/NCC mixture samples were prepared by mixing appropriate quantities of aqueous stock solutions of QHEC and NCC with distilled-deionized water. Water was purified by the Millipore Milli-Q system. The samples were stirred and left for equilibration at room temperature for 3 days. Four QHEC concentrations were used here: 1.0, 1.5, 2.0 and 3.0 wt%. At each QHEC concentration, NCC was added in the concentration range from 0 to 0.4 wt% to induce a sol–gel transition. And hereafter the sample composition was represented in the following way: c_{QHEC}/c_{NCC} (QHEC concentration/NCC concentration).

The phase behavior was determined by visual inspection. All the tested samples displayed one homogeneous phase.

2.3. Characterization

The dynamic rheological measurement of the QHEC/NCC aqueous solution was carried out on an AR-G2 rheometer (TA Instruments, USA.). Cone and plate (2° nominal angle) geometry was used to measure the dynamic oscillatory parameters. The strain used for the linear viscoelastic region was determined by performing amplitude sweep experiments at a frequency of 1 rad·s^{-1}. Temperature control was established with a ThermoCube 200/300/400 (Solid State Cooling Systems Co., USA) kept within ±0.05 °C of the desired temperature. All samples were allowed to relax for 0.5 h after the loading process, to eliminate the loading affections. In order to reduce the testing experimental error, all experiments were repeated twice.

The morphology of the NCC particles was investigated by scanning electron microscope (SEM) using a Hitachi model S-4800 apparatus (Hitachi Tokyo, Japan) equipped with a field emission source and operating at accelerating voltages of 5 kV or 30 kV (30 kV in STEM mode). For transmission electron microscope (TEM) analysis, a drop of the NCC aqueous suspension was deposited on a carbon-coated copper TEM grid for 3 min and the excess of suspension was wicked off using filter paper. The TEM grid was allowed to dry at room temperature for 3 min. The sample was then stained by depositing a drop of uranyl acetate solution (2 wt% in water) on the grid for 5 min. The excess solution was wicked off using filter paper and the grid was dried at room temperature prior to imaging.

The effective particle size of NCC particles based on translational diffusion constant was determined by dynamic light scattering (DLS). The instrument was a Zetasizer model Nano ZS from Malvern (Worcestershire, United Kingdom). The wavelength of the 4 mW He–Ne laser source was 633 nm. The particle size was measured at room temperature, and the NCC concentration was 0.1 wt%.

The zeta potential of QHEC/NCC solution was determined by Zetasizer model Nano ZS from Malvern (Worcestershire, United Kingdom). Zetasizer model Nano ZS was also a zeta potential analyzer based on electrophoretic light scatting. A 4 mW He–Ne laser source with 633 nm wavelength was used as light source. All measurements were performed at 20 °C.

3. Results and discussion

3.1. Rheological behaviors of QHEC/NCC solution

Polymeric gel is a three-dimensional network, formed from flexible chains through either chemical cross-linking or physical phase transformation. The gelation is a phenomenon in which a polymeric liquid dramatically becomes solid-like at a critical point in polymer concentration, temperature, storage time, and so forth (Lue & Zhang, 2008).Traditionally, the crossover of the storage modulus $G'(\omega)$ and loss modulus $G''(\omega)$ curves has been used as an indicator of the gel point (Tung & Dynes, 1982). This method is simple, however, frequency dependent. Valuable contributions to this area were made by the studies of chemical and physical gelations in Winter's laboratory (Chambon & Winter, 1985; Winter & Chambon, 1986; Chambon & Winter, 1987), and they generalized that

$$G'(\omega) = G''(\omega) \sim \omega^{n} 0 < n < 1 \quad (1)$$

and

$$\frac{G''(\omega)}{G'(\omega)} = \tan\delta = \tan\left(\frac{n\pi}{2}\right) \quad (2)$$

for the gelling system, where ω is the frequency, $G'(\omega)$ is the storage modulus, $G''(\omega)$ is the loss modulus, $\tan\delta$ is the loss tangent, and n is the relaxation exponent at the gel point. The frequency independence of the $\tan\delta$ in the vicinity of the gel point has been widely examined for gels and has also been employed to determine the gel

point (Lue & Zhang, 2008; Shi et al., 2012; Song, Niu, Wang, & Zhang, 2011; Madbouly, Xia, & Kessler, 2012). In the following part, Winter and Chambon theory has been applied to the mixture of oppositely charged QHEC and NCC to determine the gelation behavior and gel point.

Fig. 1 shows the storage modulus $G'(\omega)$ and loss modulus $G''(\omega)$ of the 1.0 wt% QHEC solution with various NCC concentrations as a function of angular frequency ω at 25 °C, and the c_{NCC} varied from 0 to 0.26 wt%. Both $G'(\omega)$ and $G''(\omega)$ curves increased with an increase of NCC concentration and the curves were becoming flat with smaller slope versus frequency, indicating a mutative network formation in the QHEC/NCC mixture system as NCC addition. It was noted that the dynamic mechanical behavior of the QHEC/NCC solution follows liquid-like terminal behavior at very low NCC concentrations, whereas deviation from the above relations becomes more obvious for higher c_{NCC}. When the NCC concentration was 0, the low frequency slopes of $G'(\omega)$ and $G''(\omega)$ curves have been calculated as

$$G\prime(\omega) \propto \omega^{1.41} G\prime\prime(\omega) \propto \omega^{0.98} (\omega \longrightarrow 0) \quad (3)$$

On the other hand, at the highest NCC concentration, the behavior of $G'(\omega)$ = constant at $\omega \longrightarrow 0$ was the sign of the formation of a gel plateau, according to the method by Nijenhuis and Winter (Nijenhuis & Winter, 1989). As the c_{NCC} increased, the slope of $G'(\omega)$ versus ω varied from 1.41 to near 0, whereas the slope of the $G''(\omega)$ versus ω curve lied in the range from 0.98 to near 0. Therefore, it was reasonable to consider that the sol–gel transition has occurred in the range of the slopes. The QHEC/NCC solution at other QHEC concentrations such as 1.5, 2.0, and 3.0 wt% exhibited similar behaviors so that they were not shown here.

Fig. 2 showed the tanδ value of the 1.0, 1.5, 2.0, and 3.0 wt% QHEC solutions with various NCC concentrations, respectively. It was noted that the tanδ value for all the curves decreased with an increase of NCC concentration, indicating a transition from viscose liquid to elastic solid. The tanδ value of the curve for the QHEC/NCC mixture composed of 1.0 wt% QHEC and 0.144 wt% NCC approached a plateau value close to 2.85, indicating frequency-independence in the frequency range from 0.1 to 30 rad/s. Moreover, when c_{QHEC} were 1.5, 2.0, and 3.0 wt%, the tanδ curves of the QHEC/NCC solution with c_{NCC} from 0.159 to 0.228 wt% exhibited similar behaviors, showing plateau tanδ values in the range 2.66–2.24, respectively. As shown in Fig. 2 and Table 1, at each QHEC concentration (1.0, 1.5, 2.0, and 3.0 wt%), a curve of the QHEC/NCC solution with different NCC concentration that obeyed Winter and Chambon theory in the frequency range was obtained, indicating a gel point induced by NCC addition with different concentration (0.144, 0.159, 0.184, and 0.228 wt%), and the NCC concentration was confirmed to be the gel concentration ($c_{g,NCC}$) at each c_{QHEC}, respectively. The tanδ value at each frequency-independent range gave different results from 2.85 to 2.24, and by using Eq. (2), the n values at each c_{QHEC} have been calculated from the tanδ values measured at each c_{QHEC}, to be in the range 0.785–0.733, which would be further explained in the following part. In view of the data in Fig. 1, the changes in $G'(\omega)$ and $G''(\omega)$ curves in the low-frequency range were in accordance with the power law shown in Eq. (1). $G'(\omega)$ and $G''(\omega)$ at low frequency have been selected here because they were of greater importance for the Winter and Chambon theory.

Complex viscosity (η^*) was also an important variable for the viscoelastic behavior of the gelation process. Fig. 3 showed η^* of the 1.0, 1.5, 2.0 and 3.0 wt% QHEC solutions with various NCC concentrations, respectively. At each QHEC concentration, the η^* behaved as a function of NCC concentration and increased with the NCC addition, suggesting enhancement of the electrostatic adsorption interaction between the oppositely charged macromolecules and nano-rods. Moreover, higher c_{QHEC} led to higher η^*, indicating the mixture structure and viscoelastic behavior were influenced by QHEC and NCC, as well as the association or entanglement of QHEC chains in solution. In the high-frequency range, η^* exhibited shear-thinning behaviors, while in the low-frequency range, η^* demonstrated independent of frequency, and the range of frequency independent behavior of η^* shifted to lower frequencies with an increase of c_{NCC}.

The approximate value of the zero-shear viscosity (η_0) could be obtained from the η^* at $\omega \longrightarrow 0$. Therefore, we defined the value of η^* in the frequency-independent range as η_0 (Li, Uchida, & Aoki, 1997). Fig. 4 showed η_0 obtained from Fig. 3 as a function of c_{NCC} at 1.0, 1.5, 2.0 and 3.0 wt% QHEC concentrations, respectively. The η_0 versus c_{NCC} curves showed that η_0 varied with NCC concentrations, and η_0 values increased with an increase of c_{QHEC}. At higher c_{QHEC}, more polymer chains existed, so that more association and entanglements of the polymer chains could be achieved, leading to higher viscosity. The slope of the η_0 curves reflected the sensitivity of η_0 to the NCC concentration, and it decreased with an increase in the QHEC concentration, indicating at low QHEC concentrations the NCC addition had greater influences on the mixture structure and the resultant viscoelastic property. At higher c_{QHEC}, a well-defined 3-D network was established by the larger amount of macromolecules among chain association and entanglements. However, at lower c_{QHEC}, the connection between polymer chains were loose and there could be dissociative polymer chains in the solution, therefore, electrostatic adsorption exhibited less significantly effects at higher c_{QHEC}. On the other hand, the η_0 versus c_{NCC} curves all obtained break points, and interestingly, the NCC concentrations at the breaks were 0.144, 0.159, 0.184, and 0.288 wt %, respectively, with the c_{QHEC} to be 1.0, 1.5, 2.0, and 3.0 wt%. The results were in accordance with the $c_{g,NCC}$ obtained by the frequency-independence relationships of tanδ in Fig. 2, indicating that η_0 of the system tended to diverge near its gel point.

From the data analysis in Table 1, the $c_{g,NCC}$ values increased with the elevation of c_{QHEC}, indicating that the more NCC amount needed to form a critical gel at relatively high c_{QHEC} than at low QHEC concentration, which was probably attributed to the larger amount of QHEC chains in the solution at higher concentrations. In all the tested QHEC/NCC samples, QHEC were excessive compared with NCC. In that case, in the mixture system the QHEC behaved as abundant flexible chains and NCC rods acted as junctions that connected QHEC chains with each other by electrostatic adsorption interaction, to form a 3-dimentional network. Therefore, more NCC rods were needed for more QHEC chains. From the present results, the Winter and Chambon theory has been proved to be applicable to the gelation system induced by electrostatic adsorption interaction between oppositely charged polymer solution and colloid suspension.

3.2. Behaviors of critical QHEC/NCC gels

It is well-known that the shear relaxation modulus $G(t)$ is predicted to obey a power law relaxation at the gel point (Izuka & Winter, 1992):

$$G(t) = S_g t^{-n} \quad (4)$$

Here S_g is the gel strength and has an unusual dimension of Pa·s^n. n is the relaxation exponent that determines the stress relaxation rate at the gel point, which can be calculated by Eq. (2) with the tanδ value at the critical gel point. S_g can simply be considered as the relaxation modulus at the critical gel point when the relaxation time t is 1 s. To express S_g by Eq. (4), a similar expression can be applied to $G'(\omega)$ and $G''(\omega)$ at the gel point as

$$G\prime(\omega) = \frac{G\prime\prime(\omega)}{\tan\delta} = S_g \omega^n \Gamma(1-n)\cos\left(\frac{n\pi}{2}\right) \quad (5)$$

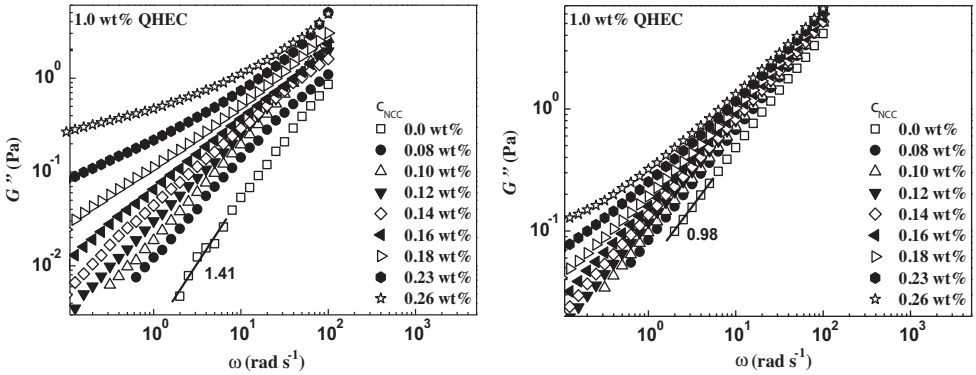

Fig. 1. Storage modulus $G'(\omega)$ and loss modulus $G''(\omega)$ of the 1.0 wt% QHEC solution with various NCC concentrations as a function of angular frequency ω at 25 °C. Values represent the slope of the line.

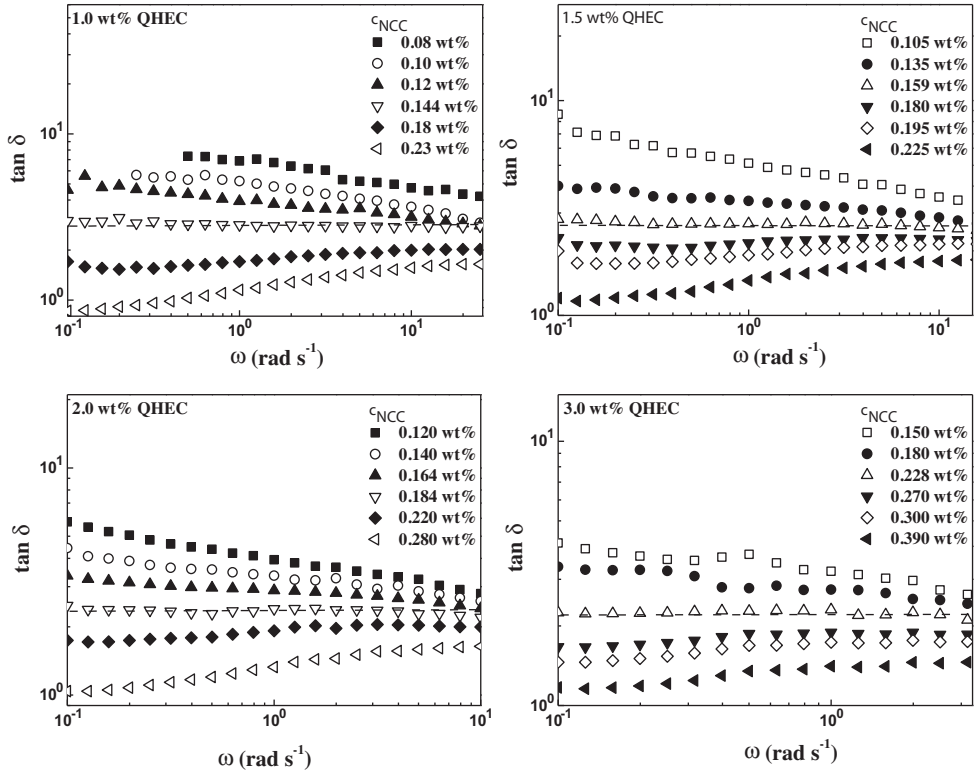

Fig. 2. tanδ of the 1.0, 1.5, 2.0, and 3.0 wt% QHEC solutions with various NCC concentrations, respectively.

Here $\Gamma(1-n)$ is the Γ function. By testing the n value at the critical gel point, we can calculate S_g from $G'(\omega)$ and $G''(\omega)$ at the gel point using Eq. (5) above.

As shown in Table 1, the n values varied with different QHEC concentrations, indicating the solution structure and viscoelastic property at the critical gel point was differed with different c_{QHEC} and $c_{g,NCC}$. Usually, the n value is not universal and varies with the gelling system. The gelation theories predicted that the value of n lies between 2/3 and 1 (Martin, Adolf, & Wilcoxon, 1988). In general, the n value is related to the physically fractal dimension, and reflects the degree of compactness of the network. A lower value of n implies the formation of a more highly elastic gel (Gao & Nishinari, 2004; Nordby, Kjøniksen, Nyström, & Roots, 2003; Kjøniksen, Hiorth, Roots, & Nysrtom, 2003). The larger tanδ

Table 1
The experimental values of critical gel concentration $c_{g,NCC}$ for the sol–gel transition, tanδ, relaxation exponent n (both from tanδ and scaling law), and gel strength S_g in the QHEC/NCC solution.

c_{QHEC} (wt%)	$c_{g,NCC}$ (wt%)	tanδ	n from tanδ	S_g (Pa·sn)	n from scaling law
1.0	0.144	2.85 ± 0.15	0.785 ± 0.009	0.0385	0.558
1.5	0.159	2.66 ± 0.14	0.771 ± 0.010	0.0924	0.627
2.0	0.184	2.41 ± 0.12	0.750 ± 0.010	0.269	0.656
3.0	0.228	2.24 ± 0.14	0.733 ± 0.013	0.996	0.734

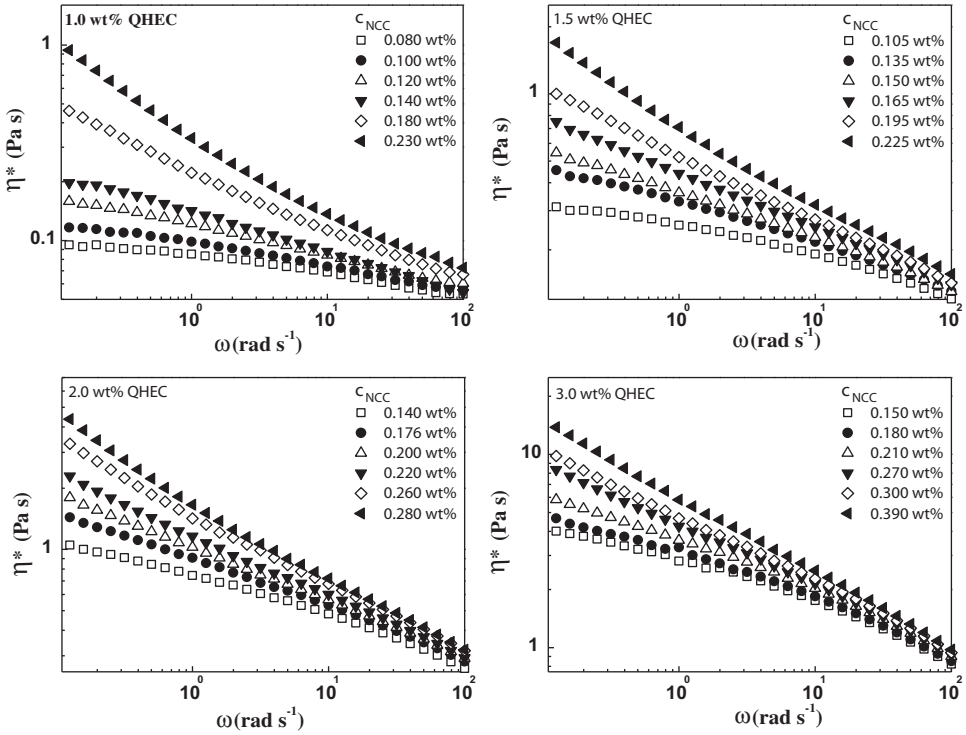

Fig. 3. η^* of the 1.0, 1.5, 2.0 and 3.0 wt% QHEC solutions with various NCC concentrations, respectively.

and n values at lower c_{QHEC} suggested a less elastic nature of the QHEC/NCC solution at the gel point, and as the c_{QHEC} increased, the solution became more elastic, leading to the decrease of both tanδ and n value. As mentioned before, since the QHEC were excessive compared to NCC, QHEC were abundant flexible chains and NCC played an important role as junctions in the networking. At higher c_{QHEC}, more polymer chains were involved in the formation of a 3-dimentional network, and the structure was denser and more compact compared with that at low c_{QHEC}, resulting in smaller n values at higher c_{QHEC}.

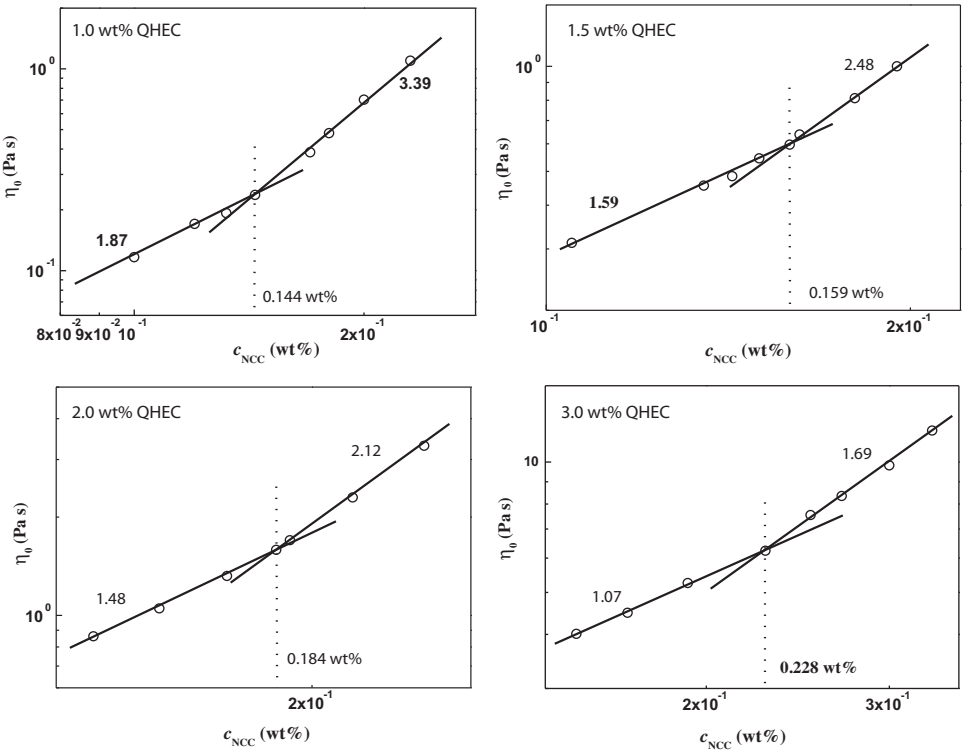

Fig. 4. η_0 obtained from Fig. 3 as a function of NCC concentration at 1.0, 1.5, 2.0 and 3.0 wt% QHEC concentrations. Value close up to the fitted line represent the slope of the line.

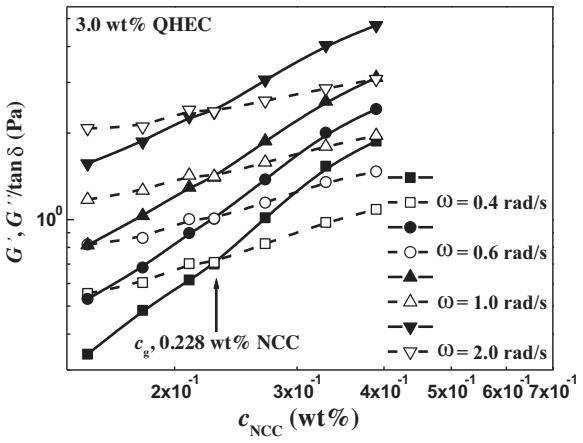

Fig. 5. Plots of G' and $G''/\tan\delta$ against the NCC concentration of 3.0 wt% QHEC solution was varied from 0.4 to 2 rad/s. The arrow indicates the gel point.

In addition, the physical nature of a gelling system at the critical gel point can be described by the S_g defined in Eqs. (4) and (5). For chemical gels, the S_g rose while n decreased, as a result of the increase of the cross-linking density, suggesting that S_g was related to the physical strength of the gel network at the gel point (Kjoniksen & Nystrom, 1996). Fig. 5 showed the plots of G' and $G''/\tan\delta$ against c_{NCC} of 3.0 wt% QHEC solution in the frequency range from 0.4 to 2 rad/s. The G' and $G''/\tan\delta$ curves of different frequency groups exhibited ascending functions with an increase of c_{NCC}. Interestingly, the intersect at the gel point lied in the same NCC concentration ($c_{g,NCC}$ = 0.228 wt%), as a result of the frequency independence of $\tan\delta$. The plots of G' and $G''/\tan\delta$ against NCC concentration at the other three QHEC concentrations displayed similar behaviors as shown in Fig. 5, and were not shown here. The $c_{g,NCC}$ values were in good agreement with that from the frequency independence of $\tan\delta$ in Fig. 2. By using any value of $G'(\omega)$ at the critical gel point according to Eq. (5), we can calculate the S_g value. The S_g values were calculated by each cross-point of the curves, and within the experimental errors. The S_g values calculated were summarized in Table 1, and also plotted in Fig. 6. S_g behaved as a linear function of n and decreased with n, indicating the QHEC/NCC solution with lower n value exhibited larger S_g, as a result of the strengthening 3-D network between QHEC and NCC. As mentioned in the former, a lower n value implies the formation of a more highly elastic gel, and it is reasonable that higher elasticity led to larger gel strength. Moreover, linear relationships was observed between S_g versus c_{QHEC} and S_g versus $c_{g,NCC}$, indicating S_g of the QHEC/NCC solution at critical gel point was directly related to the total mass of QHEC and NCC in the mixture system. At the critical gel point, a 3-dimentional network was established by both QHEC chains and NCC rods in the mixture. The results suggested that the networking was created by the electrostatic adsorption interaction between QHEC and NCC, as well as the association and entanglements of QHEC polymer chains. In that case, more polymer chains were available for the networking and self-entanglement at higher c_{QHEC}, and more NCC generated more junctions for the network, both of which would enhance the network structure, leading to a more elastic nature and lager S_g value. By summarizing the above results, three relationships can be established among $c_{g,NCC}$, c_{QHEC}, and S_g as

$$c_{g,NCC} \propto c_{QHEC},\ S_g \propto c_{QHEC},\ S_g \propto c_{g,NCC} \tag{6}$$

These relationships were responsible for the applicability of the Winter and Chambon theory to the tested QHEC/NCC solution.

3.3. Scaling law before and beyond sol–gel transition

Due to the critical nature of the sol–gel transition, transient rheological properties η_0 before the gel point, and equilibrium modulus (G_e) beyond the gel point, show a distinct scaling behavior in the vicinity of the gel point (Stauffer, Coniglio, & Adam, 1982) as

$$\eta_0 \propto \epsilon^{-\gamma} \text{for} p < p_g \tag{7}$$

$$G_e \propto \epsilon^{z} \text{for} p > p_g \tag{8}$$

Here, $\epsilon = |p_g - p|/p_g$ indicates the relative distance of a variable p departing from the sol–gel transition point p_g, and p can be the degree of cross-linking, the gelation time, the gelation temperature, the gelation concentration, and so forth. γ is the critical exponent determining the critical characteristics in the vicinity of the sol–gel transition. G_e is the quasi-equilibrium modulus, and z is the scaling exponent. The term "quasi-equilibrium" here refers to the difficulty (or sometimes impossibility) in obtaining the equilibrium modulus of a physical gel (Ferry, 1980).The values of critical exponent γ and z have been predicted by many models. Winter & Chambon, 1956 have proposed a scaling law to describe the relationship between n, z, and γ before and beyond the gel point (Chambon & Winter, 1987; Mours & Winter, 1996) as

$$n = \frac{z}{(z+\gamma)} \tag{9}$$

where n is relaxation exponent, also the scaling exponent for Eq. (2) at the critical gel point. The same expression has also been derived by Martin et al. (Martin et al., 1988). Since we have obtained the $c_{g,NCC}$ of the QHEC/NCC solution by the $\tan\delta$ frequency-independence relation, c_{NCC} was recruited to replace the variable p to calculate relative distance ϵ as

$$\epsilon = \frac{|C_{g,NCC} - C_{NCC}|}{C_{g,NCC}} \tag{10}$$

Therefore, if the critical point is known, γ and z can be directly calculated from the slope of the plot of η_0 and G_e against ϵ in log-log scale.

Fig. 7 showed η_0 as a function of the relative distance ϵ for the 1.0, 1.5, 2.0 and 3.0 wt% QHEC solutions. The linear fittings gave

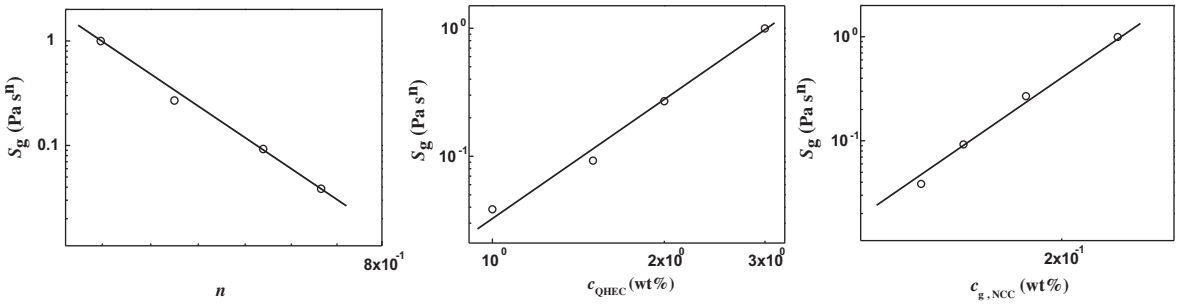

Fig. 6. S_g as a function of n, c_{QHEC} and $c_{g,NCC}$ for the QHEC/NCC solutions.

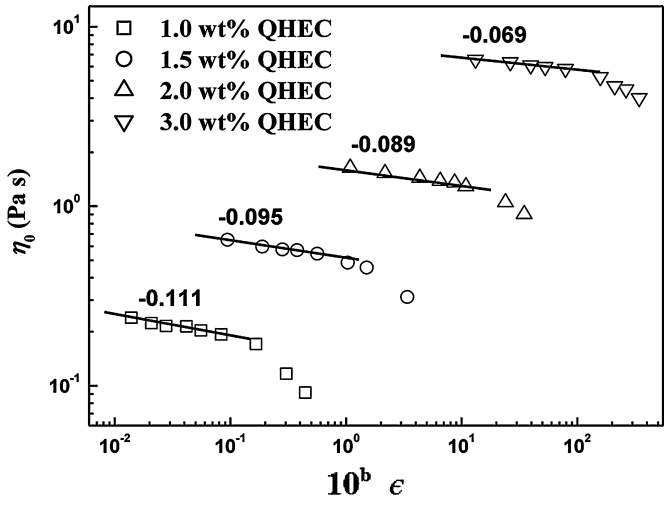

Fig. 7. η_0 as a function of the relative distance ϵ for the 1.0, 1.5, 2.0 and 3.0 wt% QHEC solutions, where the ϵ is multiplied by 10^b. The linear fittings give the solid straight lines, and the values represent the slope of the fitted lines.

the solid straight lines, and the values from -0.111 to -0.069 represented their slopes with c_{QHEC} varied from 1.0 to 3.0 wt%. Linear fit at relatively high concentrations was obtained, but discrepancy in the low concentration range was also observed. As mentioned above, η_0 was also a function of QHEC concentration. However, γ was not a constant value, and it deceased as c_{QHEC} increased. As shown in Eq. (7), γ is a parameter governing the gelation rate. In view of the data, the gelation rate was faster with lower c_{QHEC}, because of the effects of both viscosity and QHEC concentration in the mixture system.

Fig. 8 plotted G_e as a function of the relative distance ϵ for the 1.0, 1.5, 2.0 and 3.0 wt% QHEC solutions. The exponent z increased with the QHEC concentration, indicating the growth rates of the clusters were higher with relatively higher c_{QHEC}. At higher c_{QHEC}, more polymer chains were presented, and more chains were involved in the enhancement of network via electrostatic adsorption interaction with NCC addition, leading to a higher cluster growth rate at higher c_{QHEC}.

In order to validate the applicability of Eq. (9), by using our data, the n values calculated by tanδ at the critical gel point and scaling law, were also listed in Table 1. Obviously, the scaling

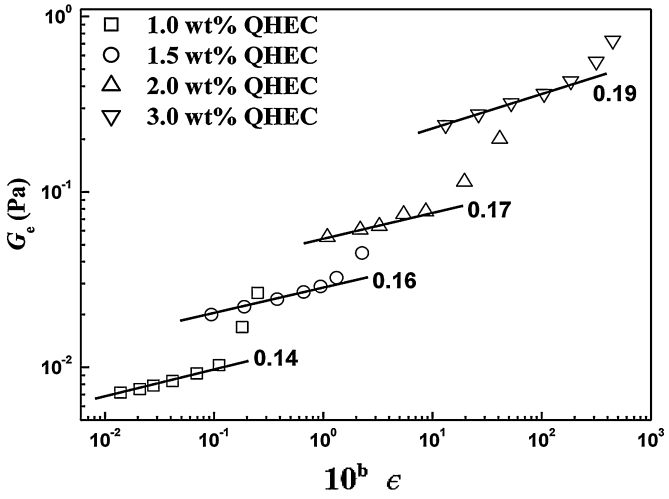

Fig. 8. G_e as a function of the relative distance ϵ for the 1.0, 1.5, 2.0 and 3.0 wt% QHEC solutions, where the ϵ is multiplied by 10^b. The linear fittings give the solid straight lines, and the values represent the slope of the fitted lines.

Table 2
Parameters obtained from QHEC/NCC mixtures at the critical gel points.

Samples	^1N (m^{-3})	d_{mesh} (nm)	$N_{agg,NCC}$
1.0 wt%/0.144 wt%	0.178×10^{21}	178	0.30
1.5 wt%/0.159 wt%	1.006×10^{21}	100	0.06
2.0 wt%/0.184 wt%	2.572×10^{21}	73	0.03
3.0 wt%/0.228 wt%	9.483×10^{21}	47	0.01

law was only feasible at in the tested solution with the highest c_{QHEC}, 3.0 wt%. Therefore, the symmetric scaling law before and beyond the gel point was only suitable for the application to the complex QHEC/NCC mixture system with high QHEC concentrations. Nemoto et al. has investigated the gelation behavior of α,ω-dihydroxyl polybutadiene/p-xylene system, and found that the intermolecular interaction, namely hydrogen bonding between hydroxyl groups at the chain ends in their case, has great influences on the application of scaling law, i. e., the scaling law worked only when the hydrogen bonding interaction in the system could be neglected (Koike, Nemoto, Watanabe, & Osaki, 1996). Moreover, in the complex cellulose solution in NaOH/thiourea, the scaling law was not feasible at higher temperatures, at which the inter- and intra-moleuclar hydrogen bonds were re-established (Lue & Zhang, 2008), indicating the intermolecular interaction could play an important role in the application of scaling law.

In the complex QHEC/NCC solution system, two effects induced the formation of a 3-dimentional network by forming junctions, leading to a sol–gel transition, namely the association and entanglement of the QHEC molecular chains as well as the electrostatic adsorption between QHEC chains and NCC rods. The former was a universal phenomenon in the polymer solution with a concentration higher than the critical overlap concentration, and the latter was presented in our system because of the oppositely charged polymer and colloid. Obviously, at higher QHEC concentrations, more polymer chains led to more associations and entanglements. The plateau value of G_0 (average of $G'(\omega)$ values at the four highest angular frequencies) allows for the calculation of a network junction density ^1N via $G_0 = {}^1Nk_BT$ with ^1N the network junction density, T the temperature, and k_B the Boltzmann's constant. This in turn can be used to calculate a mesh size $d_{mesh} = 1/{}^1N(1/3)$ and then give a rough estimation for the number of NCC rods per junction $N_{agg,NCC} = {}^1N_s/{}^1N$ with the number density of NCC rods ^1N_s (Hoffmann et al., 2011). These parameters obtained from QHEC/NCC solution at each critical gel point and pure QHEC solutions were listed in Table 2 Table 3, respectively. Take 1 wt% QHEC as an example, the network junction density of the pure 1.0 wt% QHEC solution was 0.146×10^{21}, smaller than that of the 1.0 wt% QHEC/0.144 wt% NCC at the critical gel point, indicating the addition of NCC induced electrostatic adsorption and formed more network junctions. And the d_{mesh} was also smaller in the 1.0 wt% QHEC/0.144 wt% NCC at the critical gel point than in the pure 1.0 wt% QHEC solution, suggesting the network has been tightened by the adsorption with NCC addition. The other concentrations exhibited a similar phenomenon, i.e., the addition of NCC rods led to a larger ^1N and smaller d_{mesh}, as a result of the electrostatic adsorption interaction. The number of NCC rods per junction $N_{agg,NCC}$ was calculated and the values decreased with the increase of c_{QHEC}. At critical gel point with the lowest c_{QHEC}

Table 3
Parameters obtained from QHEC solutions at different concentrations.

Samples	^1N (m^{-3})	d_{mesh} (nm)
1.0 wt% QHEC	0.146×10^{21}	190
1.5 wt% QHEC	0.817×10^{21}	122
2.0 wt% QHEC	2.109×10^{21}	78
3.0 wt% QHEC	7.724×10^{21}	50

(1.0 wt%/0.144 wt%), the $N_{agg,NCC}$ was 0.30, suggesting quantitatively the NCC rods were involved in 30% junction formation of the network, and the electrostatic adsorption has play an important role for gel formation, as well as the polymer chain association and entanglements. However, at the critical gel point with the highest c_{QHEC} (3.0 wt%/0.228 wt%), the $N_{agg,NCC}$ was only calculated to be 0.01, indicating 1% of the network junctions were composed by NCC rods. Obviously, when the c_{QHEC} was increased, according to Table 2 the $N_{agg,NCC}$ decreased, indicated that the influences of NCC rods in the gel formation was also decreasing, and the at the highest c_{QHEC} the network was dominantly composed of QHEC polymer chain association and entanglements rather than the electrostatic adsorption interaction, indicating the latter can be neglected. Therefore, the scaling law was only applicable at the highest c_{QHEC} since electrostatic adsorption interaction exhibited the weakest influences, in accordance with the results published by Nemoto (Koike et al., 1996). So far, the application of scaling law in a mixture composed of oppositely charged polymer and colloid has been verified, and the scaling law applicability has also been validated and interpreted.

4. Conclusions

Positively charged QHEC aqueous solution within the concentration range from 1.0 wt% to 3.0 wt% underwent a sol–gel transition with an addition of negatively charged NCC colloid suspension, due to the electrostatic adsorption interactions. On the basis of the results, Winter and Chambon, 1986 theory was proved to be applicable to the complex QHEC/NCC mixture system, and critical gel point have been successfully determined. With the c_{QHEC} increasing, more NCC were needed to form a critical gel, and smaller tanδ and relaxation exponent n values at the gel point were observed, indicating the elastic nature of mixture was enhanced with QHEC increase. Gel strength was a function of both c_{QHEC} and c_{NCC}, suggesting the 3-dimentional network at the critical gel point was composed of entanglements and association of QHEC macromolecular chains, as well as the electrostatic adsorption interaction between QHEC chains and NCC rods. The calculated number of NCC rods per junction was decreasing from 0.30 to 0.01 with the c_{QHEC} increased from 1.0 wt% to 3.0 wt%, indicating the electrostatic adsorption interaction between the NCC rods and QHEC chains was less significant to gel formation when increasing QHEC. Therefore, the exponents of scaling law $\eta_0 \propto \epsilon^{-\gamma}$ and $G_e \propto \epsilon^z$ for the QHEC/NCC mixtures revealed that the scaling law $n = z/(z+\gamma)$ between n, γ and z was only feasible at highest c_{QHEC}, because in that case the intermolecular interaction (electrostatic adsorption interaction in this article) was so weak that can be neglected and the critical gel network was dominated by QHEC chain entanglements and association.

Acknowledgment

The authors thank the National Institute for Nanotechnology of National Research Council of Canada for supporting this project. The work was financially supported by Alberta Innovates-BioSolutions (which includes former Alberta Forestry Research Institute) and the National Natural Science Foundation of China (51203122).

References

Azeredo, M. C. (2009). *Food Research International*, *42*, 1240–1253.
Bain, C. D., Claesson, P. M., Langevin, D., Meszaros, R., Nylander, T., Stubenrauch, C., Titmuss, S., & von Klitzing, R. (2010). *Advances in Colloid and Interface Science*, *155*, 32–49.
Beck, S., Bouchard, J., & Berry, R. (2011). *Biomacromolecules*, *12*, 167–172.
Benaissi, K., Johnson, L., Walsh, D. A., & Thielemans, W. (2010). *Green Chemistry*, *12*, 220–222.
Boluk, Y., Zhao, L., & Incani, V. (2012). *Langmuir*, *28*, 6114–6123.
Bondeson, D., Mathew, A., & Oksman, K. (2006). *Cellulose*, *13*(2), 171–180.
Chambon, F., & Winter, H. H. (1985). *Polymer Bulletin.*, *13*, 499–503.
Chambon, F., & Winter, H. H. (1987). *Journal of Rheology*, *31*, 683–697.
Czaja, W. K., Young, D. J., Kawecki, M., & Brown, R. M. (2007). *Biomacromolecules*, *8*, 1–12.
Dickinson, E. (1992). *An introduction to food Colloids*. NewYork: Oxford University Press.
Dong, S., & Roman, M. (2007). *Journal of American Chemical Society*, *129*, 13810–13811.
Ferry, J. D. (1980). *Viscoelastic properties of polymers*. New York: John Wiley & Sons.
Gao, S., & Nishinari, K. (2004). *Biomacromolecules*, *5*, 175–185.
George, M. C., Mohraz, A., Piech, M., Bell, N. S., Lewis, J. A., & Braun, P. V. (2009). *Advanced Materials*, *21*, 66–70.
Habibi, Y., Lucia, L. A., & Rojas, O. J. (2010). *Chemical Reviews*, *110*, 3479–3500.
Hoffmann, I., Heunemann, P., Prévost, S., Schweins, R., Wagner, N. J., & Gradzielski,M. (2011). *Langmuir*, *27*, 4386–4396.
Izuka, A., & Winter, H. H. (1992). *Macromolecules*, *25*, 2422–2428.
Kjøniksen, A.-L., Hiorth, M., Roots, J., & Nysrtom, B. (2003). *Journal of Physical Chemistry B*, *107*, 6324–6328.
Kjoniksen, A.-L., & Nystrom, B. (1996). *Macromolecules*, *29*, 5215–5222.
Koike, A., Nemoto, N., Watanabe, Y., & Osaki, K. (1996). *Polymer Journal*, *28*, 942–950.
Kumar, A., Dubin, P. L., Hernon, M. J., Li, Y., & Jaeger, W. J. (2007). *Journal of Physical Chemistry B*, *111*, 8468–8476.
Lam, V. D., & Walker, L. M. (2010). *Langmuir*, *26*, 10489–10496.
Larson, R. G. (1999). *The structure and rheology of complex fluids*. New York: Oxford University Press.
Li, L., Uchida, H., & Aoki, Y. (1997). *Macromolecules*, *30*, 7842–7848.
Li, Q., & Lewis, J. A. (2003). *Advanced Materials*, *15*, 1639–1643.
Liang, D., Hsiao, B. S., & Chu,B. (2007). *Advanced Drug Delivery Reviews*, *59*, 1392–1412.
Liu, D., Chen, X., Yue, Y., Chen, M., & Wu, Q. (2011). *Carbohydrate Polymers*, *84*, 316–322.
Lue, A., & Zhang, L. J. (2008). *Journal of Physical Chemistry B*, *112*, 4488–4495.
Madbouly, S. A., Xia, Y., & Kessler, M. R. (2012). *Macromolecules*, *45*, 7729–7739.
Martin, J. E., Adolf, D., & Wilcoxon, J. P. (1988). *Physical Review Letters*, *61*, 2620–2623.
Mezei, A., & Meszaros, R. (2008). *Soft Matter*, *4*, 586–592.
Moon, R. J., Martini, A., Nairn, J., Simonsenf, J., & Youngblood, J. (2011). *Chemical Society Reviews*, *40*, 3941–3994.
Mours, M., & Winter, H. H. (1996). *Macromolecules*, *29*, 7221–7229.
Nielsen, L. J., Eyley, S., Thielemans, W., & Aylott, J. W. (2010). *Chemical Communications*, *46*, 8929–8931.
Nijenhuis, K., & Winter, H. H. (1989). *Macromolecules*, *22*, 411–414.
Nordby, M. H., Kjøniksen, A.-L., Nyström, B., & Roots, J. (2003). *Biomacromolecules*, *4*, 337–343.
Otsubo, Y. (1990). *Langmuir*, *6*, 114–118.
Pan, J., Hamad, W., & Straus, S. K. (2010). *Macromolecules*, *43*, 3851–3858.
Paralikar, S. A., Simonsen, J., & Lombardi, J. (2008). *Journal of Membrane Science*, *320*, 248–258.
Pickrahn, K., Rajaram, B., & Mohraz, A. (2010). *Langmuir*, *26*, 2392–2400.
Rånby, B. G. (1949). *Acta Chemica Scandinavica*, *3*, 649–650.
Rhim, J. W. (2007). *Food Science and Biotechnology*, *16*, 691–709.
Sameer Dalvi, V., & Rajesh Dave, N. (2009). *Industrial & Engineering Chemistry Research*, *48*, 7581–7593.
Samir, M. A. S. A., Alloin, F., & Dufresne. (2005). *Biomacromolecules*, *6*, 612–626.
Shi, X., Lu, A., Cai, J., Zhang, L., Zhang, H., Li, J., & Wang, X. (2012). *Biomacromolecules*, *13*, 2370–2378.
Shin, Y., Blackwood, J. M., Bae, I. T., Arey, B. W., & Exarhos, G. J. (2007). *Materials Letters*, *61*, 4297–4300.
Siqueira, G., Bras, J., & Dufresne, A. (2010). *Polymers*, *2*, 728–765.
Siro, I., & Plackett, D. (2010). *Cellulose*, *17*(3), 459–494.
Sivakumar, S., Bansal, V., Cortez, C., Chong, S., Zelikin, A. N., & Caruso, F. (2009). *Advanced Materials*, *21*, 1820–1824.
Smay, J. E., Cesarano, J., III, & Lewis, J. A. (2002). *Langmuir*, *18*, 5429–5437.
Smay, J. E., Gratson, G. M., Shepherd, R. F., Cesarano, J., III, & Lewis, J. A. (2002). *Advanced Materials*, *14*, 1279–1283.
Song, H., Niu, Y., Wang, Z., & Zhang, J. (2011). *Biomacromolecules*, *12*, 1087–1096.
Stauffer, D., Coniglio, A., & Adam, A. (1982). *Advances in Polymer Science*, *44*, 103–158.
Tung, C. Y. M., & Dynes, P. J. (1982). *Journal of Applied Polymer Science*, *27*, 569–574.
Wang, H., & Roman, M. (2011a). *Biomacromolecules*, *12*, 3708–3714.
Wang, H., & Roman, M. (2011b). *Biomacromolecules*, *12*, 1585–1593.
Wang, J., Shaw, L. L., & Cameron, T. B. (2006). *Journal of American Ceramics Society*, *89*, 346–349.
Winter, H. H., & Chambon, F. (1986). *Journal of Rheology*, *30*, 367–382.
Woltman, S. J., Jay, G. D., & Crawford, G. P. (2007). *Nature Materials*, *6*, 929–938.
Yang, H., Tejado, Á., Alam, N., Antal, M., & van de Ven, T. G. M. (2012). *Langmuir*, *28*, 7834–7842.
Yap, H. P., Quinn, J. F., Ng, S. M., Cho, J., & Caruso, F. (2005). *Langmuir*, *21*, 4328–4333.
Ye, X., Tong, P., & Fetters, L. J. (1997). *Macromolecules*, *30*, 4103–4111.